



Deposited via The University of Leeds.

White Rose Research Online URL for this paper:

<https://eprints.whiterose.ac.uk/id/eprint/155142/>

Version: Accepted Version

Article:

Jin, H, Lin, G, Zeiny, A et al. (2019) Experimental study of transparent oscillating heat pipes filled with solar absorptive nanofluids. *International Journal of Heat and Mass Transfer*, 139. pp. 789-801. ISSN: 0017-9310

<https://doi.org/10.1016/j.ijheatmasstransfer.2019.04.117>

© 2019 Published by Elsevier Ltd.. This manuscript version is made available under the CC-BY-NC-ND 4.0 license <http://creativecommons.org/licenses/by-nc-nd/4.0/>.

Reuse

This article is distributed under the terms of the Creative Commons Attribution-NonCommercial-NoDerivs (CC BY-NC-ND) licence. This licence only allows you to download this work and share it with others as long as you credit the authors, but you can't change the article in any way or use it commercially. More information and the full terms of the licence here: <https://creativecommons.org/licenses/>

Takedown

If you consider content in White Rose Research Online to be in breach of UK law, please notify us by emailing eprints@whiterose.ac.uk including the URL of the record and the reason for the withdrawal request.

Experimental study of transparent oscillating heat pipes filled with solar absorptive nanofluids

Haichuan Jin¹ Guiping Lin¹ Lizhan Bai¹ Jinjing Cai¹ Dongsheng Wen^{1,2,*}

¹ Laboratory of Fundamental Science on Ergonomics and Environmental Control, School of Aeronautic Science and Engineering, Beihang University, Beijing 100191, PR China

² School of Chemical and Process Engineering, University of Leeds, Leeds, LS2 9JT, UK

Abstract: Nanoparticle-based volumetric solar absorption has been shown to be an effective technique to realize efficient solar harvesting. However, most of such systems under study are stationary and cannot realize solar energy transport, which limits their potential applications to a large extent. A novel idea of using directive absorptive nanofluids in oscillating heat pipes (OHP) is investigated in this work, which would achieve efficient solar energy capture and transportation simultaneously without the use of any additional pumping power. The influence of a variety of parameters such as nanoparticle type, nanoparticle concentration, nanofluids filling ratio and solar radiation intensity on the performance of OHPs are investigated. There exists an optimal filling ratio of the nanofluid for the OHP (i.e., 83%), under which single direction circulation of the working fluid is observed, where the thermal resistance of the OHP reaches the minimum. The OHP reaches an extremely high thermal conductivity, i.e., 6000 W/(m · K), when filled with 3.0 wt% MWCNT nanofluid. The maximum energy conversion efficiency has been observed as much as 92% for the current experimental settings. It is found that strong absorption of solar energy, efficient vapor generation inside the OHP and proper configuration of the OHP should be responsible for the efficient operation of this system.

Keywords: solar energy, nanoparticle, volumetric solar harvesting, oscillating heat pipe

* Corresponding authors. Tel.: +86 10 8231 7528; Fax: +86 10 8233 8600

E-mail addresses: d.wen@buaa.edu.cn (D. Wen)

1 **Nomenclature**

2	A	surface area exposed to solar radiation (m^2)
3		absorbance (-)
4	c	specific heat capacity ($J/(kg \cdot K)$)
5	c_p	specific heat capacity at constant pressure ($J/(kg \cdot K)$)
6	D	particle diameter (m)
7	D_i	the diameter of OHP tube (m)
8	E	spectral emissive power (W/m^3)
9	EF	effective thermal conductivity ratio (-)
10	f_v	volume concentration (-)
11	I	radiative intensity (W/m^2)
12	k	thermal conductivity ($W/(m \cdot K)$)
13	k_f	imaginary part of the complex refractive index of the based fluid (-)
14	L	optical depth (m)
15	m	mass (kg)
16		relative refractive index (-)
17	n	complex refractive index (-)
18	Q	heat flux (W/m^2)
19		efficiency factor for Rayleigh scattering approximation (-)
20	R	radius of OHP tube (m)

1		thermal resistance coefficient (K/W)
2	r	radius in the integrating process (m)
3	T	temperature ($^{\circ}C$)
4	t	time (s)
5	U	uncertainty (-)
6	x	characteristic size of nanoparticles (-)
7		<i>Greek symbols</i>
8	η	efficiency (-)
9	κ	absorption coefficient (m^{-1})
10	σ	surface tension coefficient (N/m)
11	λ	wavelength of light in vacuum (m)
12	ρ	density (kg/m^3)
13		<i>Superscripts</i>
14	-	average value
15		<i>Subscripts</i>
16	<i>abs</i>	absorption
17	<i>adia</i>	adiabatic
18	<i>amb</i>	ambient
19	<i>b</i>	black body
20	<i>c</i>	condenser
21	<i>e</i>	evaporator

1	f	fluid
2	η	wavelength range
3	I	radiative intensity
4	<i>liq</i>	liquid
5	n	nanoparticle
6	p	particle
7	<i>sca</i>	scattering
8	s	scattering
9	<i>vap</i>	vapor
10	w	water
11	<i>Abbreviations</i>	
12	AuNPs	gold (Au) nanoparticles
13	DI	deionized
14	MWCNT	multiwall carbon nanotube
15	OHP	oscillating heat pipe
16	PTE	photothermal conversion efficiency
17	RTE	radiative transfer equation
18	SAR	specific absorption rate
19	SEM	scanning electron microscope
20	TC	thermocouple
21	TEM	transmission electron microscopy

1 UV ultraviolet

2 UCD Ultrasonic Cell Disruption system

3

4

1 **1 Introduction**

2 Developing renewable and sustainable energy technologies, especially solar energy related, is
3 of great importance to secure our energy future [1,2]. Among different solar applications such as
4 photovoltaics and photocatalysis, solar thermal system still occupies the largest share [3]. However,
5 for current solar thermal systems, the big challenge lies in the energy conversion efficiency. For
6 example, in conventional solar thermal collectors, engineered surface is utilized as the solar
7 absorber where solar radiation is converted into heat, and then heat is transferred to a working fluid
8 flowing in the tubes embedded within or welded onto the surface. In such a system, the efficiency
9 is limited by not only how efficiently the solar absorber captures the solar radiation, but also how
10 effectively the heat is transferred to the working fluid [4]. It is a traditional surface-controlled heat
11 transfer process with relatively high thermal resistance, in which the highest temperature is on the
12 absorber surface and the lowest temperature is in the center of the fluids [5,6], resulting in poor
13 energy efficiency especially under high solar concentrations (>100). There are two obvious
14 shortcomings for this system: first, the energy conversion efficiency from solar radiation to the
15 internal energy of the working fluid is limited, because the heat loss from the solar absorber where
16 it has the highest temperature, leading to high radiation loss; Secondly, additional pump power is
17 needed to circulate the fluid, which further increases the energy expense for the system.

18 In order to enhance the energy conversion efficiency of solar thermal collectors, nanoparticle-
19 based direct absorption concept has been proposed [2,7–9], which makes use of particular
20 nanoparticles dispersed in the base fluid to realize effective solar photo-thermal conversion.
21 Comparing to traditional solar thermal collectors, not only the base fluid absorbing solar energy,
22 the dispersed nanoparticles could convert the solar energy to heat directly within the base fluid and
23 transfer the heat to the base fluid efficiently. Such an idea transfers the surface heat transfer

1 limitation associated with conventional solar thermal collectors into a volumetric absorption
2 process, which can increase the solar energy conversion efficiency significantly by properly
3 engineering solar absorption spectrum at the nanoscale [10–14]. Many experimental studies have
4 been conducted since this concept was first proposed. For example, the solar photothermal
5 conversion efficiency of a 0.01% graphite nanofluid was found to be as high as 122.7% of that of
6 a conventional surface absorbing collector [15]. Some metallic nanoparticles such as gold and
7 silver have also drawn wide attentions because of their Surface Plasmon Resonance effects (SPR)
8 [15–17]. For these kinds of materials, the resonance frequencies of conduction electrons are
9 usually in the visible-light spectrum , which is weakly absorbed by most of the heat transfer fluids
10 but occupies nearly half of the total solar radiation energy [18]. SPR-induced intensive absorption
11 of radiative energy (i.e., even leading to vapor generation) has shown excellent photo-thermal
12 conversion capabilities [19]. Zhang et al. [9] showed that a very low concentration of gold
13 nanoparticles (i.e., mass concentration of 0.0028%) could increase the photo-thermal conversion
14 efficiency (PTE) of the base fluid by 20%, and reached an impressive specific absorption rate
15 (SAR) ~ 10 kW/g under laboratory conditions. In another study conducted outdoor, up to 144%
16 enhancement in the stored solar thermal energy was obtained for 6.0.01 wt% silver nanoparticle-
17 based direct absorption under natural sunlight conditions [8].

18 In order to realize pump-free thermal energy transport, oscillating heat pipe (OHP) is a good
19 candidate. As a promising heat transfer concept first proposed in the 1990's [20], OHP has the
20 advantage of simple structure, low cost, high flexibility and excellent heat transfer performance
21 [21–23]. OHP is made of a long capillary tube bent into many turns, and fluid circulation is driven
22 by bubble expansion at the evaporator section and contraction at the condenser section, without
23 the requirement of additional pumping power [24,25]. Currently in some OHP studies, capillary

1 tubes are made of metals [26–29] and some are made of transparent materials [30–32] for ‘flow
2 visualization’ purpose. However, solar irradiation is not the direct heat source for almost all these
3 studies, and the heat from the heat source is transferred to the working fluid by conduction only.

4 To allow direct usage of solar energy by OHP technology, a novel idea of employing transparent
5 glass capillary tubes to allow direct heating of the fluid at the evaporation section is proposed in
6 this work. This new idea combines the advantages of OHP based phase change technology and
7 direct absorptive nanofluids technology, and would achieve efficient solar energy capture and
8 transportation simultaneously without the use of any additional pumping power. An experimental
9 study is conducted in this work to validate the new concept. Different transparent OHPs with
10 nanoparticle dispersions as the working fluid for direct solar absorption were fabricated. Extensive
11 experimental studies were carried out, including the influence of the fluid charging ratio, the OHP
12 geometries n, cooling type of condenser, type of nanoparticle, nanoparticle concentration and solar
13 intensity. Thermal resistance of OHPs were calculated, it was found that adding nanoparticles
14 could significantly improve the thermal conductivity of OHP. The maximum thermal conductivity
15 reached $6000 \text{ W}/(\text{m} \cdot \text{K})$ when the OHP was filled with 3.0 wt% MWCNT nanofluid. There was
16 an optimal filling ratio of the nanofluid, at which quasi-sine oscillation of wall temperature could
17 be established. The proposed concept can efficiently harvest solar energy and spontaneously
18 transfer the heat into targeted areas, providing a novel approach for efficient solar energy
19 utilization.

20

21 **2 Experimental system**

22 2.1 Preparation of AuNPs and MWCNT nanofluids

1 Au nanoparticles (AuNPs) and Multi-Walled Carbon Nanotubes (MWCNT) have been reported
2 to have strong solar absorption, and they were selected for the preparation of different nanofluids
3 as the working fluids of the OHP. The one-step method [33] was employed to produce stable
4 AuNPs nanofluids. Briefly 5×10^{-6} mol HAuCl₄ was first dispersed into 190 ml DI water in a three-
5 necked flask. A magnetic blender with a heating source was used to stir the liquid until boiling.
6 Boiling was continued for 10 mins and 10 ml of 0.5% sodium citrate was subsequently added. The
7 solution turned dark blue within 30 s and the final color became wine red after being heated for an
8 additional 20 mins. The dispersions maintained good stability for over two months and were used
9 for the experiments without further purification and separation. Particles' size and shape were
10 characterized (**Fig. 1A**) by a Transmission Electron Microscopy (TEM) (Tecnai G2 F20 S-TWIN).

11 The two-step method [8] was used to produce stable MWCNT nanofluids. MWCNT powder
12 was purchased from Beijing DK Nano Technology Co., LTD. First, the powder was dispersed into
13 deionized water (DI water) and put into an ultrasonic bath (ThermoFisher Scientific, FB11207) for
14 30 min. Second, the dispersion solution was processed by an Ultrasonic Cell Disruption (UCD)
15 system (ThermoFisher Scientific, FB705) with 50% power for 2 hours. The size and shape of the
16 MWCNTs were characterized by a Scanning Electron Microscopy (SEM) (JEM-1200EX) (**Fig.**
17 **1B**) and TEM (**Fig. 1C**).

18 The nanofluids before experiment were processed by UCD System with 50% power for 2 hours.
19 After that, the nanofluids were standing for 2 months and tested by a UV-spectrophotometer
20 (Shimadzu UV-1800) to compare the changes in absorption. The difference of absorbance before
21 and after standing for 2 months was less than 1%, which indicated an excellent stability.

22 2.2 Experimental setup and data acquisition

1 In order to realize volumetric solar absorption, the pipe wall of the OHP was made of high-
 2 temperature resistant quartz glass, which can allow almost all the sunlight to pass through. Two
 3 types of OHP were used in the experiments, one with the gap of 1.5 mm between two adjacent
 4 pipes (**Fig. 1D**) and the other with nearly no gap (**Fig. 1E**). Each OHP had six turns, and the pipes
 5 were numbered by 1 to 12 from left to right in sequence in order to present the temperature
 6 distribution from infrared images. The average temperature of pipe number 1, 2, 11, 12 is named
 7 as **Edge 1**. The average temperature of pipe number 3, 4, 9, 10 is named as **Edge 2**. The average
 8 temperature of pipe number 5~8 is named as **Center**. With regard to the inner diameter (Di) range
 9 of OHPs, it is determined by the following empirical equations [34]:

$$10 \quad Di_{min} \leq Di \leq Di_{max} \quad (1-a)$$

$$11 \quad Di_{min} = 0.7 \sqrt{\frac{\sigma}{(\rho_{liq} - \rho_{vap})g}} \approx 1.78 \text{ mm} \quad (1-b)$$

$$12 \quad Di_{max} = 1.84 \sqrt{\frac{\sigma}{(\rho_{liq} - \rho_{vap})g}} \approx 5.24 \text{ mm} \quad (1-c)$$

13 where ρ_{liq} , ρ_{vap} , σ and g are the density of liquid and vapor, the surface tension of working fluid
 14 and the gravitational acceleration, respectively. Both types of OHPs had the same inner diameter
 15 of 2 mm and the length of pipes of 200 mm (**Fig. 1E**). In order to make the sunlight illuminating
 16 perpendicularly to the OHPs, the angle of the OHPs is oriented as 45°. In order to investigate the
 17 influence of cooling type at the condenser section on the thermal behavior of the OHP, the
 18 experiments were arranged for 3 groups (**Fig. 2**) and 10 cases (**Table 1**). As shown in **Fig. 3**, two
 19 Fresnel lenses (Shenzhen MEIYING Technology CO., LTD.) with a 50 cm and 100 cm focal
 20 distance were used to focus the sunlight with 220 times and 500 times, respectively. A vacuum
 21 pump (Leybold, D16C) was employed for filling the OHP with the working fluid. An infrared
 22 camera (Fluke Tix 640 with 30 mm lens) with precision of $\pm 0.1^\circ\text{C}$ was used to capture the

1 temperature distribution and variation of the OHPs. In order to record the bubble generation and
2 increase process, a high-performance camera (Canon 70D with 18-135 mm lens) was employed.
3 Three type K thermocouples with precision of $\pm 0.1^\circ\text{C}$ (Omega 5TC-TT-K-30-36) were connected
4 to a data acquisition system (National Instruments PIXe-1073). Two of the thermocouples were
5 used to measure the temperature change of water with thermal insulation for cooling the condenser
6 of the OHP (**Fig. 3B**). One thermocouple was used to measure the ambient temperature change
7 during the experiment. A solar radiation intensity sensor with a measurement uncertainty of 2.0%
8 was employed to measure the solar intensity.

9 All the experiments were conducted on 30th April 2017 (location: 39° 59' 5.49" North, 116° 21'
10 18.70" East) from 10.00 am to 15.00 pm. As shown in **Fig. 4**, The solar intensity varied from
11 870~1000 W/m², the ambient temperature varied from 33~38 °C during the experiment, which
12 was relatively stable for the current experimental setting.

13 **3 Results and discussions**

14 3.1 Effect of nanofluids

15 In order to compare the performance of the OHP charged with AuNPs nanofluid with that
16 charged with DI water, a series of controlled experiments were carried out in sequence (i.e., filling
17 with DI water and 0.01 wt% AuNPs, filling ratio of 75%), as shown in **Fig. 5**. For the same filling
18 ratio, the operating temperature of the OHP charged with 0.01 wt% AuNPs nanofluid was
19 obviously higher than that filled with DI water, indicating that AuNPs nanofluid can enhance the
20 photo-thermal conversion efficiency due to the effect of volumetric absorption, consistent with our
21 previous conclusions [6]. From infrared images, it can be seen that the operating temperature of
22 the OHP charged with nanofluid was obviously higher. The OHP filled with AuNPs nanofluid can
23 absorb more solar energy than that filled with DI water, leading to more bubble generation and

1 tempestuous circulation. Faster vapor bubble generation and condensation will transfer more
2 energy and lower the thermal resistance significantly. The temperature distribution in the
3 evaporator section is more uniform when filled with AuNPs nanofluid than that filled with DI
4 water, due to strong absorption of solar energy and enhanced circulation of the working fluid inside
5 the OHP. During the experiment, no nanoparticles aggregation can be visually observed in the
6 vapor bubble inside OHP. The concentration of Au nanofluid and MWCNT nanofluid has been
7 measured through the UV-spectrophotometer (i.e., to compare the absorbance of nanofluid) before
8 and after experiment. The result shows that the concentration maintains the same before and after
9 experiment, which demonstrates that no sedimentation of nanoparticles during the OHP operating.

10 3.1 Quasi-sine oscillating behavior

11 In order to investigate the quasi-sine oscillating behavior of the operating temperature of OHPs,
12 both infrared images and photos from high speed camera were captured for AuNP nanofluid, as
13 shown in **Fig. 6**. At the beginning, the temperature of the OHP is approximately the same as the
14 ambient temperature (i.e., ~30 °C). After the application of solar radiation, the temperature of the
15 OHP at the solar heating area increased dramatically and non-uniformly. 20 seconds later, the
16 high temperature zone of the OHP extended gradually, and some working fluid with relatively
17 high temperature reached the top of the OHP. 30 seconds later, a sudden temperature drop of
18 center tubes happened (which can be seen from

19 **Fig. 7C**), indicating that some working fluid from the condenser section (with relatively low
20 temperature) should reach the solar heating area. 40 seconds later, the temperature of the OHP at
21 the heating area increased continuously until a dramatic temperature drop happens 10 seconds
22 later, which was consistent with the temperature variation trend in

1 **Fig. 7C.** In

2 **Fig. 7C**, the operating temperature of the OHP exhibited an obvious quasi-sine oscillating mode,
3 which is closely associated with the oscillating motion of the working fluid inside the OHPs.

4
5 3.2 Effect of filling ratio

6 The filling ratio is defined as the ratio of liquid working fluid volume to the total volume of the
7 OHP. Using AuNP nanofluids (0.024 wt%) as an example, the influence of filling ratio on the
8 thermal performance of the OHP was investigated (

9 **Fig. 7**). When the filling ratio was relatively small, i.e., 42% in

10 **Fig. 7A**, most AuNPs nanofluid was suspended at the condenser section. The reason is that once
11 the nanofluid entered the evaporator section, it was evaporated immediately due to the strong
12 absorption of solar radiation. The quick vapor generation phenomenon was carefully investigated
13 in our previous study [35]. The large amount of vapor caused the nanofluid to suspend in the
14 upside, which was difficult to flow downward to the solar heating area to absorb the solar energy
15 again. The final result was that the OHP was operating weakly, leading to relatively high
16 temperature at the evaporator, and the oscillating frequency was low, as shown in

17 **Fig. 7A.**

18 With the increase of filling ratio, the operation of the OHP became more stable and the
19 oscillating frequency became higher, as shown in

20 **Fig. 7B** and **C**. What's more, when the filling ratio reached a certain value (e.g., 67%), single
21 direction circulation of the working fluid was observed, as clearly observed from both camera and

1 infrared videos, which was evidenced by the large temperature difference between adjacent pipes.
2 With intensive solar irradiation at the evaporator section, fluid seeded with AuNPs would be
3 evaporated quickly, and the generated vapor bubbles forced the fluid to go up into the condenser
4 section, where they were condensed by water cooling. The condensed liquid was forced to run
5 downward in another adjacent pipe, resulting in lower temperature in this pipe (i.e., almost the
6 same temperature as the cooling water). The OHP with higher filling ratio could realize higher
7 solar energy absorption than that with the lower filling ratio because more evaporator section was
8 occupied by liquid working fluid. The higher filling ratio of nanofluid will also lower the thermal
9 resistance between the evaporator and condenser and can convert (i.e., transfers) more solar energy
10 into thermal form. Further investigation on the thermal resistance and heat flux is discussed later.

11 Due to the fact that the relative number of liquid slugs and vapor plugs depends on the filling
12 ratio, it has a significant influence on the performance of the OHP. Han et.al [21] reviewed many
13 previous studies [36–38] and concluded that there was an “optimal range” for the filling ratio,
14 which was generally recommended as 35%-65%. However, the optimal filling ratio in this work
15 shows a big difference. It seems that the optimal filling ratio is higher than 65%, reaching 83% or
16 even more. Due to the direct absorption of solar irradiation and consequently heat loss reduction,
17 the absorbed solar flux in this work is much higher than the energy input in previous studies (i.e.,
18 as much as 40 W/cm^2 for AuNPs nanofluid, 140 W/cm^2 for MWCNTs). Higher heat flux
19 concentrated in the evaporator section will evaporate the liquid much faster and lead to the dry-
20 out phenomenon more easily, which requires more liquid to replenish the evaporator. Clearly
21 increasing energy flux will increase the optimum filling ratio for the OHP [21].

22 With a very low filling ratio, the evaporator section of the OHP would possibly be dried out
23 easily, leading to poor running performance (e.g.,

1 **Fig. 7A**), which is consistent with many previous researches [34,39]. However, with the increase
2 of the filling ratio, a quasi-sine oscillation [40] pattern of the wall temperature was observed (
3 **Fig. 7B, C**). It was observed that these sinusoidal waves originated from regular oscillating
4 motions were available only at suitable power inputs and filling ratios. With the increase of power
5 input, the working fluid started to move irregularly, resulting in irregular fluctuations of bubble
6 displacement or velocity. Actually, both experimental and modeling investigations [41–43]
7 showed that the oscillating motions in OHPs were essentially chaotic, suggesting the absence of
8 long-term periodic or quasi-periodic oscillating motions. Recently, the dynamic behavior
9 comparisons of vapor columns or bubbles under pulse and continuous heating by Xian et al. [44]
10 demonstrated that both the displacement and velocity of front and end of vapor columns were
11 highly irregular. From the experiments as shown in **Fig. 6**, it was observed that the quasi-sine
12 oscillation was only observed in the OHP when the filling ratio was higher than 67%.

13

14 3.4 Thermal resistance in different cases

15 In order to investigate the thermal resistance of the OHP in different cases, the photothermal
16 conversion efficiency of AuNPs nanofluids with different concentrations and DI water has to be
17 theoretically calculated. According to our previous study [35], nanoparticles inside the nanofluids
18 should scatter the sunlight independently, and the absorption and scattering coefficients could be
19 calculated based on Mie scattering theory. In the present modeling, the characteristic size of a
20 nanoparticle was represented by $\alpha = \pi D / \lambda$, where D is the diameter of the nanoparticle, about
21 20nm characterized by TEM, and λ is the wavelength of radiation. As the diameter of
22 nanoparticles is far smaller than the wavelength of irradiation ($\alpha \ll 1$), a simplified Rayleigh

1 scattering approximation [45] was used to calculate the extinction coefficient of the nanoparticles,
 2 as shown below:

$$3 \quad Q_a(\lambda) = 4\alpha \operatorname{Im} \left\{ \frac{m^2 - 1}{m^2 + 2} \left[1 + \frac{\alpha^2}{15} \left(\frac{m^2 - 1}{m^2 + 2} \right) \frac{m^4 + 27m^2 + 38}{2m^2 + 3} \right] \right\} \quad (2-a)$$

$$4 \quad Q_s(\lambda) = \frac{8}{3} \alpha^4 \left| \frac{m^2 - 1}{m^2 + 2} \right|^2 \quad (2-b)$$

$$5 \quad Q_e(\lambda) = Q_a(\lambda) + Q_s(\lambda) \quad (2-c)$$

$$6 \quad \kappa(\lambda) = \kappa_p(\lambda) + \kappa_f(\lambda) = \frac{3\pi}{2} \frac{f_v Q_{abs}(\lambda)}{D} + \frac{4\pi k_f(\lambda)}{\lambda} \quad (2-d)$$

7 where $Q_e(\lambda)$, $Q_a(\lambda)$ and $Q_s(\lambda)$ are the extinction, absorption and scattering factors, respectively;
 8 $\kappa(\lambda)$ is the absorption coefficient of Au nanofluid, f_v is the volume concentration of AuNPs
 9 nanofluid, κ_f is the absorption coefficient of pure water, and m represents the relative complex
 10 refractive index of nanofluid, calculated by:

$$11 \quad m = \frac{n_{particles}}{n_{fluid}} \quad (2-e)$$

12 where $n_{particles}$ and n_{fluid} are the complex refractive indexes of gold and base fluid (water),
 13 respectively. The efficiency factors of gold nanoparticle with diameter of 20 nm can be seen in
 14 **Fig. 8**. Compared with the absorption factor, the scattering factor of gold nanoparticle is very small.
 15 As the scattering factor is proportional to the 4th order of α and $\alpha \ll 1$, it is much smaller than the
 16 absorption factor. In terms of energy conversion, the scattering part is not considered when
 17 calculating the photothermal conversion efficiency for solar thermal harvesting.

1 The photothermal conversion efficiency of the OHP can be calculated through the equation
 2 below, which integrates the efficiency with the radius of the cylindrical solar receiver, as:

$$3 \quad \eta(f_v) = \frac{\int_0^R \int_{0.2\mu\text{m}}^{3\mu\text{m}} E_0(\lambda) (1 - e^{-2\kappa(\lambda, f_v)r}) d\lambda dr}{R \int_{0.2\mu\text{m}}^{3\mu\text{m}} E_0(\lambda) d\lambda} \quad (3)$$

4 where E represents the spectral emissive power (as shown in **Fig. 9A**), η is the photo-thermal
 5 conversion efficiency.

6 The absorbed solar energy by the OHP can be calculated as:

$$7 \quad Q_{abs} = \eta_{f_v} \eta_l I S_l \quad (4)$$

8 where η_l is efficiency of Fresnel lens ($\eta_l \approx 95\%$, which was measured by the experiment), I is the
 9 solar intensity in the experiment (measured by solar intensity sensor, as seen in **Fig. 4**), S_l is the
 10 area of the Fresnel lens.

11 The thermal resistance of the OHP can be calculated from [46]:

$$12 \quad R_{OHP} = \frac{\bar{T}_e - \bar{T}_c}{Q_{abs}} \quad (5-a)$$

13 where \bar{T}_e and \bar{T}_c are the average temperatures of the evaporator and condenser, respectively.

14 Based on the standard error analysis method [47], the uncertainty for the thermal resistance can
 15 be expressed as:

$$16 \quad \frac{U_{R_{OHP}}}{R_{OHP}} = \sqrt{2 \left(\frac{U_T}{\bar{T}_e - \bar{T}_c} \right)^2 + \left(\frac{U_I}{I} \right)^2} \quad (5-b)$$

17 Where $U_{R_{OHP}}$ is the uncertainty of thermal resistance. U_T and U_I are the uncertainty of temperature
 18 and solar intensity, which are from the infrared camera and solar intensity sensor. The uncertainty
 19 analysis shows that $\frac{U_{R_{OHP}}}{R_{OHP}}$ is less than 5%, so the error bar is not shown in the figures related. In
 20 order to check the repeatability and reproducibility of the experiments, each experiment were
 21 conducted twice and the final calculated thermal resistance maintains within 5% deviation.

1 The thermal resistance in different cases (**Table 1**) changing with the filling ratio is shown in
2 **Fig. 9B**. For the OHP with 2 mm gap between two adjacent pipes (**CASE D** and **CASE E**), heat
3 pipe filled with the nanofluid (i.e., 0.01 wt% AuNPs) has smaller thermal resistance than that filled
4 with DI water. There is a minimum thermal resistance when the filling ratio reaches a certain value
5 (e.g., 0.38 K/W at the filling ratio of 92% for the OHP filled with AuNPs, 0.99 K/W at the filling
6 ratio of 75%). What's more, the OHP filled with the nanofluid can significantly reduce the thermal
7 resistance, as much as 24% for **CASE E** compared with **CASE D**. That is because nanofluids can
8 not only absorb much more solar energy but also enhance the bubble formation process, which has
9 been widely investigated through boiling and evaporation phenomenon. Filling more working fluid
10 can decrease the thermal resistance (i.e., enhance the performance of the OHP), but when the filling
11 ratio reaches 100%, the thermal resistance jumps dramatically (due to safety consideration,
12 running time was very short to avoid physical damage of the OHP. The steady state temperature
13 difference should be much larger than that in **Fig. 9B** for the filling ratio of 100%, leading to a
14 much higher thermal resistance value). This finding is in consistence with the video where the
15 oscillating becomes much stranger when the filling ratio is much higher and stops when the
16 working fluid fully fills the OHP.

17 However, increasing the volume concentration of AuNPs nanofluids not only increases the heat
18 flux transferred from the evaporator to condenser but also increases the temperature of the
19 evaporator. As a result, the thermal resistance may maintain at the same level (e.g., the thermal
20 resistance of **CASE B** almost the same as that of **CASE C** for different filling ratios. The
21 concentration is 0.01 wt% and 0.024 wt%, respectively).

22 What's interesting is about the thermal resistance of the OHP in **CASE F** and **CASE G**. The
23 thermal resistance of the OHP when the condenser is cooled by natural air is averagely smaller

1 than those in other cases. In fact, the cooling performance of natural air convection is very poor,
2 which results in an obviously higher operating temperature, and the temperature difference
3 between the evaporator and condenser corresponding to the same pressure drop becomes smaller
4 due to increased saturation pressure/temperature slope of the working fluid, leading to relatively
5 small thermal resistance.

6

7 3.5 Energy conversion efficiency

8 In order to study how much solar energy can the OHP collect and transport, the OHP filled with
9 DI water (**CASE H**) and 0.024 wt% AuNPs nanofluid (**CASE I**) whose condenser section was
10 immersed in a water tank with good thermal insulation were tested (The filling ratio is 83%). The
11 water temperature variation is shown in **Fig. 10**. 60 minutes later, for the OHP filled with DI water,
12 the water temperature increase is about 20 °C, while it is about 40 °C for the OHP filled with 0.024
13 wt% AuNPs nanofluid, which is twice of that for the OHP filled with DI water. For both cases,
14 the heating power first increases dramatically, reaching the maximum value, and then decreasing
15 gradually. According to **Eq. 3-4**, the maximum heating power for the OHP filled with DI water
16 and 0.024 wt% AuNPs nanofluid is about 26W and 40 W, respectively.

17 In order to investigate the OHP filled with a high concentration of MWCNT nanofluid, another
18 experiment was carried out (**CASE J**), and the filling ratio is 83%. The variations of the
19 temperatures of the OHP evaporator and the water in the tank, heating power and thermal
20 resistance are shown in **Fig. 11**. Amazingly, the water in the tank with thermal insulation reached
21 its boiling point (i.e., 100°C) in less than 30 minutes through the heating by the OHP under
22 concentrated solar radiation (i.e., 500 suns), which can be seen from **Supplementary Material**.
23 The maximum heating power of the OHP reached 240 W, almost ten times of that of the OHP

1 filled with DI water. The temperature variations of the evaporator and the water in the tank showed
2 the same trend and reached the maximum value simultaneously (~ 27 minutes later). The
3 temperature increase of the evaporator would inevitably increase the heat leak to the surroundings,
4 and that is the main reason why the heating power decreased as the operating temperature increased.

5 Tanshen et al. [48] investigated the optimum concentration of MWCNTs solutions charged in
6 the OHPs and found that the optimum concentration for their cases was 0.2 wt%. The thermal
7 resistance of OHP suffers from the high concentration of MWCNTs, which was mainly attributed
8 to the physical characteristics of MWCNTs. The higher volumetric ratio of MWCNTs and the
9 surface characteristics provide highly viscous fluid that does not allow the fluid to move freely
10 with the same power supplied in the evaporator section. As they investigated, a higher
11 concentration than 0.3wt% would increase the thermal resistance and make it higher even than that
12 filled with water. For the case in this work, the concentration of MWCNTs nanofluid reached as
13 much as 3.0 wt%, which also increased the viscosity of the working fluid in the OHP dramatically.
14 However, the performance of the OHP was much better than that filled with water, and even higher
15 than that filled with 0.01 wt% and 0.024 wt% AuNPs nanofluids, although it has been
16 demonstrated in many researches that gold nanofluid has remarkable photothermal conversion
17 performance and solar vapor generation ability [6,9,35,49]. Actually, the main factors dominating
18 the performance in our volumetric absorption OHP is the input power (i.e., the absorbance of solar
19 energy) and the steam (i.e., bubbles) generation which can formulate the vapor plugs and liquid
20 slugs and cause the oscillatory motion. Due to a remarkable enhancement of photothermal
21 conversion efficiency and steam generation efficiency of AuNPs nanofluid, the thermal resistance
22 of the OHP filled with AuNPs nanofluids decreases and the oscillating intensity is enhanced. More
23 frequent vapor bubbles generation and condensation will accelerate the oscillating frequency and

1 as a result, transferring more solar energy to the condenser section. However, the inner diameter
 2 of the OHP must be small enough (e.g., 2 mm in this paper) so that vapor plugs and liquid slugs
 3 can be formulated due to the dominant effect of the surface tension of the working fluid, which
 4 seriously limits the absorbance of solar energy for the OHP. For instance, the photo-thermal
 5 conversion efficiency (PTE) in this work is 8.57%, 19.03% and 29.83% for the OHP filled with
 6 DI water, 0.01 wt% and 0.024 wt% nanofluids with the filling ratio of 100%, respectively, which
 7 means that most of the solar energy will penetrate the OHP due to thin optical depth.

8 According to our previous study [6], PTE is very sensitive when the optical depth is below 20
 9 mm, where PTE increases quickly with increasing optical depth. For an optical depth of 2 mm (i.e.,
 10 the diameter of the tube), the PTE for a pure fluid is in a very small range (< 10%), which
 11 significantly limits the performance of the OHP. As a result, increasing the concentration of the
 12 nanofluid becomes a desirable solution. The PTE increases with the increase of nanoparticle
 13 concentration. At a concentration of 3.0 wt% MWCNT nanofluid with a filling ratio of 100%, the
 14 PTE can reach as much as 95.3%, three times more than that of 0.024 wt% AuNPs nanofluid and
 15 over ten times more than that of DI water. With such large amount of solar energy absorbed by the
 16 OHP, the vapor bubbles can be generated immediately, and the oscillating vapor plugs and liquid
 17 slugs move quite frequently, leading to a single direction running.

18 It shall be noted that an increase of particle concentration will increase the effective viscosity,
 19 which might retard the movement of the bubbles. For any future applications, the balance of
 20 increased pressure drop and enhance PTE shall be carefully considered.

21 The effective thermal conductivity of the OHP can be calculated using the following equation[34]:

$$22 \quad k_{eff} = \frac{4L_{adia}}{n \cdot \pi \cdot D_o^2} \frac{P}{(\bar{T}_e - \bar{T}_c)} \quad (6-a)$$

$$23 \quad P = C_p m_w \frac{\Delta T_w}{\Delta t} \quad (6-b)$$

$$1 \quad U_P = C_p m_w \frac{U_T}{\Delta t} \quad (6-c)$$

$$2 \quad \frac{U_{k_{eff}}}{k_{eff}} = \sqrt{\left(\frac{U_T}{\Delta T_w}\right)^2 + 2\left(\frac{U_T}{\bar{T}_e - \bar{T}_c}\right)^2} \quad (6-d)$$

3 where L_{adia} is the length of adiabatic section (i.e., 80 mm for this case), D_o is the outer diameter
 4 of the OHP (i.e., 3 mm), n is the number of pipes, P is the heating power calculated from **Eq.6-b**
 5 (sensible increasing rate of water with insulation treatment), C_p is the specific heat of water, m_w
 6 is the mass of the water (600 g for this case). The EF [34] can directly reflect the heat transfer
 7 enhancement degree of the OHP, which is defined below:

$$8 \quad EF = \frac{k_{eff}}{k_s} \quad (7)$$

9 where $k_s = 1.39 \text{ W}/(\text{m} \cdot \text{K})$ at $T = 50 \text{ }^\circ\text{C}$ is the thermal conductivity of the substrate material
 10 (quartz glass in this work).

11 The thermal conductivity of the OHP filled with MWCNT nanofluid is shown in **Fig. 11**. The
 12 thermal conductivity reaches as much as nearly $6000 \text{ W}/(\text{m} \cdot \text{K})$, which is almost 4300 times of
 13 the thermal conductivity of substrate material (quartz glass) (i.e., $EF = 4316.5$). The thermal
 14 conductivity of the OHP filled with MWCNTs is much higher than those reported in most of the
 15 previous studies [34,39,50–52], e.g., $500\text{-}3000 \text{ W}/(\text{m} \cdot \text{K})$ from Zhao's investigation [52].

16 In order to investigate the energy conversion, harvested solar energy by OHP calculated
 17 according to the sensible heat of water-cooling condensation section of OHP. The harvested solar
 18 energy can be calculated by the following equation:

$$19 \quad Q_t = C_p m_w \Delta T_w \quad (8-a)$$

$$20 \quad U_{Q_t} = C_p m_w U_T \quad (8-b)$$

21 The converted solar energy of OHP filled with DI water, gold nanofluid and MWCNTs nanofluid
 22 can be seen in **Fig. 12A**. For OHP filled with DI water, the maximum harvested solar energy is ~

1 40 KJ in 30 minutes, and for OHP filled with gold nanofluid, the maximum absorbed solar energy
 2 is ~78 KJ. Seeding gold nanoparticles into the water can significantly increase the harvested solar
 3 energy. What's more, OHP filled with MWCNTs nanofluid with mass concentration of 3.0 wt%
 4 harvests 220 KJ solar energy in 30 minutes, which is almost 5.5 times of that of OHP filled with
 5 DI water.

6 The final energy conversion efficiency of OHP can be calculated by the following equation:

$$7 \quad \eta_t = \frac{Q_t}{I\eta_0 t} \quad (9-a)$$

$$8 \quad \frac{U\eta_t}{\eta_t} = \sqrt{\left(\frac{UQ_t}{Q_t}\right)^2 + \left(\frac{U_I}{I}\right)^2} \quad (9-b)$$

9 where S_f , η_0 are the area and optical efficiency of Fresnel Lens, respectively.

10 The energy conversion efficiency can be seen in **Fig. 12B**. The maximum efficiency of OHP
 11 filled with MWCNTs nanofluid is around 92%, which is ~9 times of that of DI water (i.e., ~10%).
 12 The reason for that could be possible: very less sunlight energy can penetrate the pipe (i.e., most
 13 of the solar energy is trapped inside the OHP) and such huge energy inside the evaporation section
 14 of OHP can shorten the need time of startup process and lead to a quasi-sine oscillating behavior
 15 of OHP, which can benefit the performance of OHP. However, the efficiency decreases after 5
 16 minutes for OHP filled with MWCNTs nanofluid, which is possibly due to increased heat loss
 17 caused by high temperature of evaporation and adiabatic section, where no thermal insulation
 18 treatment has been carried out. According to the previous discussion, the efficiency can be
 19 increased even the concentration of nanofluid is not very high if the diameter of OHP tube is
 20 increased to a certain value when the optical depth is favorable for harvesting solar energy.

21 The efficiency in this paper reaches 92% when the OHP is filled with MWCNTs, which is much
 22 higher than those reported the maximum solar thermal efficiency of a plate solar collector with
 23 glazed copper OHP. Two independent work showed that the maximum efficiency were 62% [53]

1 and 53.79% [50] respectively. This high efficiency is due to a few reasons, including 1) high heat
2 transfer process under concentrated solar intensity, where the OHP progresses intensively and
3 achieves an effective thermal conductivity of $6000 \text{ W}/(\text{m} \cdot \text{K})$; 2) low level of heat leak due to
4 the volumetric absorption of nanofluid inside the OHP by the ‘thermal trapping’ effect [6,54], i.e.,
5 the highest temperature exists inside the nanofluid instead of on the surface for plate solar
6 collectors; and 3) the compact arrangement of transparent OHP tubes that absorb most of the solar
7 energy, more efficient than most of vacuum-tube solar collector (i.e., there is a certain gap between
8 the adjacent vacuum-tube, which wastes nearly 30% of the irradiated area).

9 The energy efficiency decreases at low energy intensity, which is consistent with the results in
10 **Fig. 9B**, where CASE B under 500 sun has lower thermal resistance than that of CASE B under
11 250 sun, which means energy efficiency is at low level when solar intensity is low. This may limit
12 the application of this new technology to high solar intensity where strong bubble generation
13 phenomenon can be produced. Comparing to plate solar collectors or vacuum-tube solar collectors,
14 the proposed new idea is easier to implement and has lower cost, in addition to the efficiency issue,
15 which may warrant its certain applications.

16 **4 Conclusions**

17 In this work, transparent OHPs filled with AuNPs and MWCNT nanofluids were fabricated and
18 experimentally studied, in order to realize efficient solar energy collection and transport
19 simultaneously. A series of experiments have been conducted, some important conclusions have
20 been reached as summarized below:

- 21 ■ The classical quasi-sine oscillating behavior for the operating temperature of the OHP was
22 observed in the experiment, under appropriate filling ratio and volume concentration of the
23 nanofluids.

- 1 ■ There existed an optimal filling ratio of the nanofluid for the OHP (i.e., 83%), under which
2 single direction circulation of the working fluid was observed, where the thermal resistance
3 of the OHP reached the minimum.
- 4 ■ The addition of Au or MWCNT nanoparticles into water can significantly increase the solar
5 energy capture of the OHP via volumetric absorption. An increase of nanofluid concentration
6 not only led to more solar energy capture, but also decreased the thermal resistance of the
7 OHP. Only 24% of the thermal resistance was observed when the OHP was filled with 0.01
8 wt% Au nanofluid compared with that of the OHP filled with water.
- 9 ■ The OHP filled with 3.0 wt% MWCNT nanofluid reached an extremely high thermal
10 conductivity, i.e., $6000 \text{ W}/(\text{m} \cdot \text{K})$, which is almost 4300 times of the thermal conductivity of
11 the substrate material (quartz glass). Under this condition, the cooling water for the condenser
12 started boiling under concentrated solar radiation (500 suns) in 30 minutes.
- 13 ■ The maximum energy conversion efficiency reached 92% for OHP filled with 3.0 wt%
14 MWCNTs nanofluid.
- 15 ■ The enhanced performance was due to strong absorption of solar energy, efficient vapor
16 generation inside the OHP and proper configuration of the OHP. Further investigation should
17 be focused on the optimization of pipe geometry to increase the energy efficiency for OHPs
18 filled with a low concentration of nanofluid.

19

20 **Acknowledgements**

21 This work was supported by the National Natural Science Foundation of China (No. 51776012
22 and No.51876006), China Scholarship Council (No. 201506020031) and the EU Marie Curie
23 Actions-International Incoming Fellowships (FP7-PEOPLE-2013-IIF-913576).

1 **References**

- 2 [1] S.P. Sukhatme, Solar thermal power generation, *J. Chem. Sci.* 109 (1997) 521–531.
3 doi:10.1007/BF02869211.
- 4 [2] H.K. Gupta, G. Das Agrawal, J. Mathur, An experimental investigation of a low
5 temperature Al₂O₃-H₂O nanofluid based direct absorption solar collector, *Sol. Energy.*
6 118 (2015) 390–396. doi:10.1016/j.solener.2015.04.041.
- 7 [3] C. Maurer, C. Cappel, T.E. Kuhn, Progress in building-integrated solar thermal systems,
8 *Sol. Energy.* (2016). doi:10.1016/j.solener.2017.05.065.
- 9 [4] A. Lenert, E.N. Wang, Optimization of nanofluid volumetric receivers for solar thermal
10 energy conversion, *Sol. Energy.* 86 (2012) 253–265. doi:10.1016/j.solener.2011.09.029.
- 11 [5] G. Ni, N. Miljkovic, H. Ghasemi, X. Huang, S. V. Boriskina, C. Te Lin, J. Wang, Y. Xu,
12 M.M. Rahman, T.J. Zhang, G. Chen, Volumetric solar heating of nanofluids for direct
13 vapor generation, *Nano Energy.* 17 (2015) 290–301. doi:10.1016/j.nanoen.2015.08.021.
- 14 [6] H. Jin, G. Lin, L. Bai, M. Amjad, E.P. Bandarra Filho, D. Wen, Photothermal conversion
15 efficiency of nanofluids: An experimental and numerical study, *Sol. Energy.* 139 (2016)
16 278–289. doi:10.1016/j.solener.2016.09.021.
- 17 [7] J.E. Minardi, H.N. Chuang, Performance of a “black” liquid flat-plate solar collector, *Sol.*
18 *Energy.* 17 (1975) 179–183. doi:10.1016/0038-092X(75)90057-2.
- 19 [8] F.E.P. Bandarra, O.S.H. Mendoza, C.L.L. Beicker, A. Menezes, D. Wen, Experimental
20 investigation of a silver nanoparticle-based direct absorption solar thermal system, *Energy*
21 *Convers. Manag.* 84 (2014) 261–267. doi:10.1016/j.enconman.2014.04.009.

- 1 [9] H. Zhang, H.J. Chen, X. Du, D. Wen, Photothermal conversion characteristics of gold
2 nanoparticle dispersions, *Sol. Energy*. 100 (2014) 141–147.
3 doi:10.1016/j.solener.2013.12.004.
- 4 [10] V. Khullar, H. Tyagi, N. Hordy, T.P. Otanicar, Y. Hewakuruppu, P. Modi, R.A. Taylor,
5 Harvesting solar thermal energy through nanofluid-based volumetric absorption systems,
6 *Int. J. Heat Mass Transf.* 77 (2014) 377–384.
7 doi:10.1016/j.ijheatmasstransfer.2014.05.023.
- 8 [11] M.M. Rahman, S. Mojumder, S. Saha, S. Mekhilef, R. Saidur, Effect of solid volume
9 fraction and tilt angle in a quarter circular solar thermal collectors filled with CNT-water
10 nanofluid, *Int. Commun. Heat Mass Transf.* 57 (2014) 79–90.
11 doi:10.1016/j.icheatmasstransfer.2014.07.005.
- 12 [12] A.J. Moghadam, M. Farzane-Gord, M. Sajadi, M. Hoseyn-Zadeh, Effects of CuO/water
13 nanofluid on the efficiency of a flat-plate solar collector, *Exp. Therm. Fluid Sci.* 58 (2014)
14 9–14. doi:10.1016/j.expthermflusci.2014.06.014.
- 15 [13] G. Colangelo, E. Favale, A. De Risi, D. Laforgia, A new solution for reduced
16 sedimentation flat panel solar thermal collector using nanofluids, *Appl. Energy*. 111
17 (2013) 80–93. doi:10.1016/j.apenergy.2013.04.069.
- 18 [14] Q. He, S. Wang, S. Zeng, Z. Zheng, Experimental investigation on photothermal
19 properties of nanofluids for direct absorption solar thermal energy systems, *Energy*
20 *Convers. Manag.* 73 (2013) 150–157. doi:10.1016/j.enconman.2013.04.019.

- 1 [15] Z. Luo, C. Wang, W. Wei, G. Xiao, M. Ni, Performance improvement of a nanofluid solar
2 collector based on direct absorption collection (DAC) concepts, *Int. J. Heat Mass Transf.*
3 75 (2014) 262–271. doi:10.1016/j.ijheatmasstransfer.2014.03.072.
- 4 [16] J. Pérez-Juste, I. Pastoriza-Santos, L.M. Liz-Marzán, P. Mulvaney, Gold nanorods:
5 Synthesis, characterization and applications, *Coord. Chem. Rev.* 249 (2005) 1870–1901.
6 doi:10.1016/j.ccr.2005.01.030.
- 7 [17] S. Eustis, M.A. El-Sayed, Why gold nanoparticles are more precious than pretty gold:
8 Noble metal surface plasmon resonance and its enhancement of the radiative and
9 nonradiative properties of nanocrystals of different shapes, *Chem. Soc. Rev.* 35 (2006)
10 209–217. doi:10.1039/B514191E.
- 11 [18] G. Thuillier, M. Hersé, D. Labs, T. Foujols, W. Peetermans, D. Gillotay, P.C. Simon, H.
12 Mandel, The solar spectral irradiance from 200 to 2400 nm as measured by the SOLSPEC
13 spectrometer from the ATLAS and EURECA missions, *Sol. Phys.* 214 (2003) 1–22.
14 doi:10.1023/A:1024048429145.
- 15 [19] Z. Fang, Y.R. Zhen, O. Neumann, A. Polman, F.J. García De Abajo, P. Nordlander, N.J.
16 Halas, Evolution of light-induced vapor generation at a liquid-immersed metallic
17 nanoparticle, *Nano Lett.* 13 (2013) 1736–1742. doi:10.1021/nl4003238.
- 18 [20] H. Akachi, United States Patent: 4921041-Structure of a heat pipe, 1990.
- 19 [21] X. Han, X. Wang, H. Zheng, X. Xu, G. Chen, Review of the development of pulsating
20 heat pipe for heat dissipation, *Renew. Sustain. Energy Rev.* 59 (2016) 692–709.
21 doi:10.1016/j.rser.2015.12.350.

- 1 [22] J. Qu, X. Li, Y. Cui, Q. Wang, Design and experimental study on a hybrid flexible
2 oscillating heat pipe, *Int. J. Heat Mass Transf.* 107 (2017) 640–645.
3 doi:10.1016/j.ijheatmasstransfer.2016.11.076.
- 4 [23] Q. Sun, J. Qu, X. Li, J. Yuan, Experimental investigation of thermo-hydrodynamic
5 behavior in a closed loop oscillating heat pipe, *Exp. Therm. Fluid Sci.* 82 (2017) 450–458.
6 doi:10.1016/j.expthermflusci.2016.11.040.
- 7 [24] J. Qu, Q. Wang, Experimental study on the thermal performance of vertical closed-loop
8 oscillating heat pipes and correlation modeling, *Appl. Energy.* 112 (2013) 1154–1160.
9 doi:10.1016/j.apenergy.2013.02.030.
- 10 [25] X. Liu, Y. Chen, Fluid flow and heat transfer in flat-plate oscillating heat pipe, *Energy*
11 *Build.* 75 (2014) 29–42. doi:10.1016/j.enbuild.2014.01.041.
- 12 [26] A.A. Hathaway, C.A. Wilson, H.B. Ma, Experimental Investigation of Uneven-Turn
13 Water and Acetone Oscillating Heat Pipes, *J. Thermophys. Heat Transf.* 26 (2012) 115–
14 122. doi:10.2514/1.T3734.
- 15 [27] C.Y. Tseng, K.S. Yang, K.H. Chien, M.S. Jeng, C.C. Wang, Investigation of the
16 performance of pulsating heat pipe subject to uniform/alternating tube diameters, *Exp.*
17 *Therm. Fluid Sci.* 54 (2014) 85–92. doi:10.1016/j.expthermflusci.2014.01.019.
- 18 [28] K.H. Chien, Y.T. Lin, Y.R. Chen, K.S. Yang, C.C. Wang, A novel design of pulsating
19 heat pipe with fewer turns applicable to all orientations, *Int. J. Heat Mass Transf.* 55
20 (2012) 5722–5728. doi:10.1016/j.ijheatmasstransfer.2012.05.068.

- 1 [29] S. Rittidech, N. Pipatpaiboon, S. Thongdaeng, Thermal performance of horizontal closed-
2 loop oscillating heat-pipe with check valves, *J. Mech. Sci. Technol.* 24 (2010) 545–550.
3 doi:10.1007/s12206-009-1221-7.
- 4 [30] H. Xian, W. Xu, Y. Zhang, X. Du, Y. Yang, Experimental investigations of dynamic fluid
5 flow in oscillating heat pipe under pulse heating, *Appl. Therm. Eng.* 88 (2015) 376–383.
6 doi:10.1016/j.applthermaleng.2014.12.019.
- 7 [31] J. Qu, H. Wu, P. Cheng, Start-up, heat transfer and flow characteristics of silicon-based
8 micro pulsating heat pipes, *Int. J. Heat Mass Transf.* 55 (2012) 6109–6120.
9 doi:10.1016/j.ijheatmasstransfer.2012.06.024.
- 10 [32] J.L. Xu, Y.X. Li, T.N. Wong, High speed flow visualization of a closed loop pulsating
11 heat pipe, *Int. J. Heat Mass Transf.* 48 (2005) 3338–3351.
12 doi:10.1016/j.ijheatmasstransfer.2005.02.034.
- 13 [33] H. Chen, D. Wen, Ultrasonic-aided fabrication of gold nanofluids, *Nanoscale Res. Lett.* 6
14 (2011) 198. doi:10.1186/1556-276X-6-198.
- 15 [34] J. Qu, J. Zhao, Z. Rao, Experimental investigation on the thermal performance of three-
16 dimensional oscillating heat pipe, *Int. J. Heat Mass Transf.* 109 (2017) 589–600.
17 doi:10.1016/j.ijheatmasstransfer.2017.02.040.
- 18 [35] H. Jin, G. Lin, L. Bai, A. Zeiny, D. Wen, Steam generation in a nanoparticle-based solar
19 receiver, *Nano Energy.* 28 (2016) 397–406. doi:10.1016/j.nanoen.2016.08.011.

- 1 [36] J. Qu, H. Wu, P. Cheng, Experimental Study on Thermal Performance of a Silicon-Based
2 Micro Pulsating Heat Pipe, ASME 2009 Second Int. Conf. Micro/Nanoscale Heat Mass
3 Transf. Vol. 3. 3 (2009) 629–634. doi:10.1115/MNHMT2009-18525.
- 4 [37] W. Qu, B. Yang, Performances of Flat Plate Pulsating Heat Pipes, ASME 2009 Second
5 Int. Conf. Micro/Nanoscale Heat Mass Transf. Vol. 3. (2009) 403–410.
6 doi:10.1115/MNHMT2009-18358.
- 7 [38] Y. Yang, H. Xian, D. Liu, C. Chen, X. Du, Investigation on the Feasibility of Oscillating-
8 Flow Heat Pipe Applied in the Solar Collector, Int. J. Green Energy. 6 (2009) 426–436.
9 doi:10.1080/15435070903227896.
- 10 [39] H. Kargar Sharif Abad, M. Ghiasi, S. Jahangiri Mamouri, M.B. Shafii, A novel integrated
11 solar desalination system with a pulsating heat pipe, Desalination. 311 (2013) 206–210.
12 doi:10.1016/j.desal.2012.10.029.
- 13 [40] G. Spinato, N. Borhani, B.P. D’Entremont, J.R. Thome, Time-strip visualization and
14 thermo-hydrodynamics in a Closed Loop Pulsating Heat Pipe, Appl. Therm. Eng. 78
15 (2015) 364–372. doi:10.1016/j.applthermaleng.2014.12.045.
- 16 [41] S.M. Pouryoussefi, Y. Zhang, Numerical investigation of chaotic flow in a 2D closed-loop
17 pulsating heat pipe, Appl. Therm. Eng. 98 (2016) 617–627.
18 doi:10.1016/j.applthermaleng.2015.12.097.
- 19 [42] Y. Song, J. Xu, Chaotic Behavior of Pulsating Heat Pipes, Int. J. Heat Mass Transf. 52
20 (2009) 292–294.

- 1 [43] J. Qu, H. Wu, P. Cheng, X. Wang, Non-linear analyses of temperature oscillations in a
2 closed-loop pulsating heat pipe, *Int. J. Heat Mass Transf.* 52 (2009) 3481–3489.
3 doi:10.1016/j.ijheatmasstransfer.2009.03.012.
- 4 [44] H. Xian, W. Xu, Y. Zhang, X. Du, Y. Yang, Experimental investigations of dynamic fluid
5 flow in oscillating heat pipe under pulse heating, *Appl. Therm. Eng.* 88 (2015) 376–383.
6 doi:10.1016/j.applthermaleng.2014.12.019.
- 7 [45] M.F. Modest, *Radiative Heat Transfer*, Academic Press, 2003.
8 doi:http://dx.doi.org/10.1016/B978-012503163-9/50021-7.
- 9 [46] T. Hari Prasad, P.R. Kukutla, P. Mallikarjuna Rao, R.M. Reddy, Experimental
10 Investigation on Performance of Pulsating Heat Pipe, *ASME 2015 Gas Turbine India*
11 *Conf.* 45 (2015) V001T04A005. doi:10.1115/GTINDIA2015-1362.
- 12 [47] R.J. Moffat, Describing the uncertainties in experimental results, *Exp. Therm. Fluid Sci.* 1
13 (1988) 3–17. doi:10.1016/0894-1777(88)90043-X.
- 14 [48] M.R. Tanshen, B. Munkhbayar, M.J. Nine, H. Chung, H. Jeong, Effect of functionalized
15 MWCNTs/water nanofluids on thermal resistance and pressure fluctuation characteristics
16 in oscillating heat pipe, *Int. Commun. Heat Mass Transf.* 48 (2013) 93–98.
17 doi:10.1016/j.icheatmasstransfer.2013.08.011.
- 18 [49] O. Neumann, A.S. Urban, J. Day, S. Lal, P. Nordlander, N.J. Halas, Solar vapor
19 generation enabled by nanoparticles, *ACS Nano.* 7 (2013) 42–49. doi:10.1021/nn304948h.

- 1 [50] M. Arab, M. Soltanieh, M.B. Shafii, Experimental investigation of extra-long pulsating
2 heat pipe application in solar water heaters, *Exp. Therm. Fluid Sci.* 42 (2012) 6–15.
3 doi:10.1016/j.expthermflusci.2012.03.006.
- 4 [51] J. Qu, X. Li, Q. Wang, F. Liu, H. Guo, Heat transfer characteristics of micro-grooved
5 oscillating heat pipes, *Exp. Therm. Fluid Sci.* 85 (2017) 75–84.
6 doi:10.1016/j.expthermflusci.2017.02.022.
- 7 [52] J. Zhao, J. Qu, Z. Rao, Experiment investigation on thermal performance of a large-scale
8 oscillating heat pipe with self-rewetting fluid used for thermal energy storage, *Int. J. Heat
9 Mass Transf.* 108 (2017) 760–769. doi:10.1016/j.ijheatmasstransfer.2016.12.093.
- 10 [53] K.B. Nguyen, S.H. Yoon, J.H. Choi, Effect of working-fluid filling ratio and cooling-
11 water flow rate on the performance of solar collector with closed-loop oscillating heat
12 pipe, *J. Mech. Sci. Technol.* 26 (2012) 251–258. doi:10.1007/s12206-011-1005-8.
- 13 [54] H. Jin, G. Lin, L. Bai, A. Zeiny, D. Wen, Steam generation in a nanoparticle-based solar
14 receiver, *Nano Energy.* 28 (2016) 397–406. doi:10.1016/j.nanoen.2016.08.011.
- 15

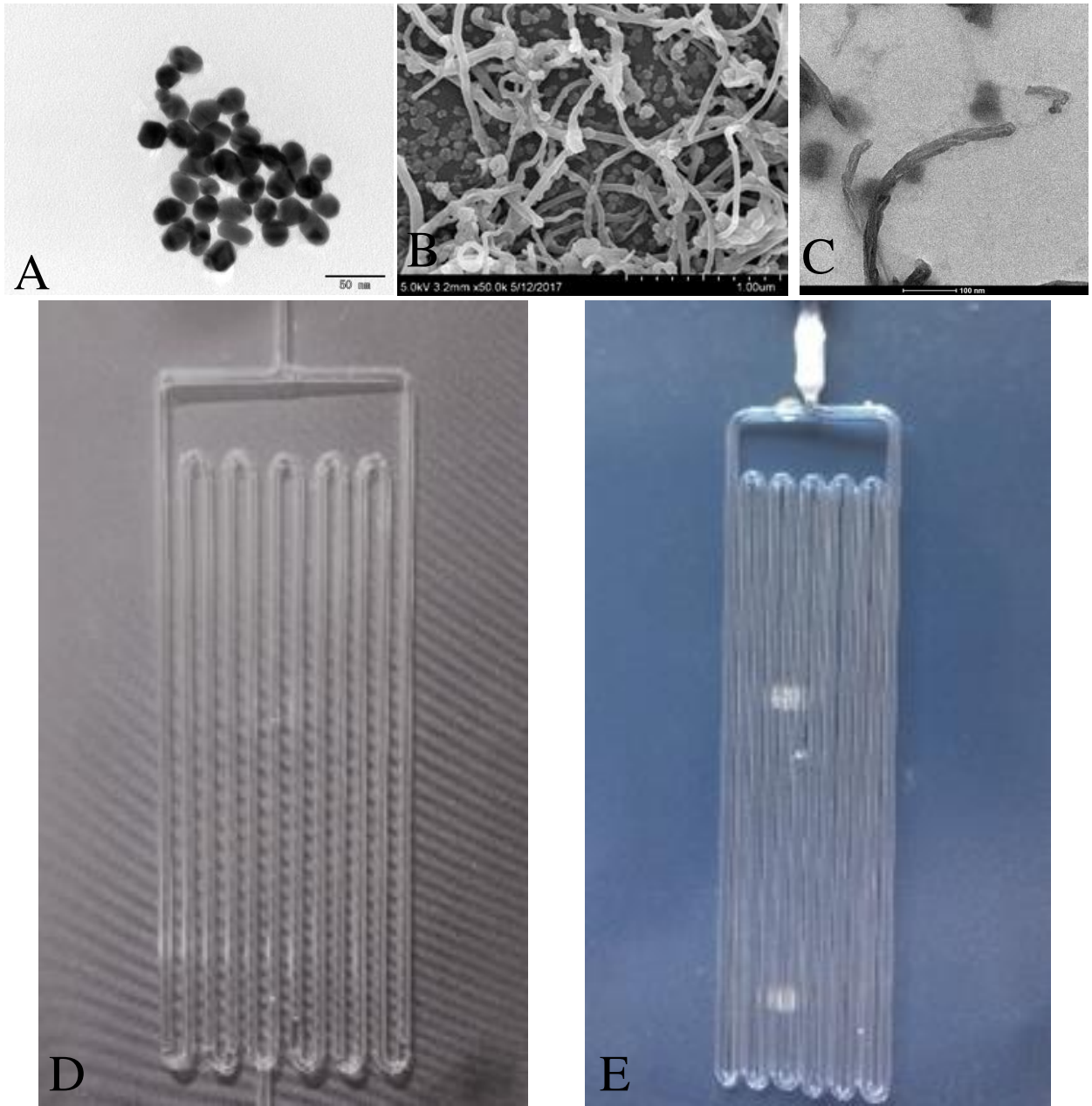
1
2
3
4
5
6
7
8
9
10
11
12

Table 1 Different cases in the experiments

Case	Gap between two adjacent pipes	Cooling type of Condenser	Working fluid	Solar intensity
A	0	15 °C cooling water	water	500 Sun
B	0	15 °C cooling water	0.01 wt% AuNPs	500 Sun
C	0	15 °C cooling water	0.024 wt% AuNPs	500 Sun
D	1.5 mm	5 °C cooling water	water	250 Sun
E	1.5 mm	5 °C cooling water	0.01 wt% AuNPs	250 Sun
F	0	natural air convection	water	500 Sun
G	0	natural air convection	0.01 wt% AuNPs	500 Sun
H	0	water tank with insulation	water	500 Sun
I	0	water tank with insulation	0.024 wt% AuNPs	500 Sun
J	0	water tank with insulation	3.0 wt% MWCNT	500 Sun

13

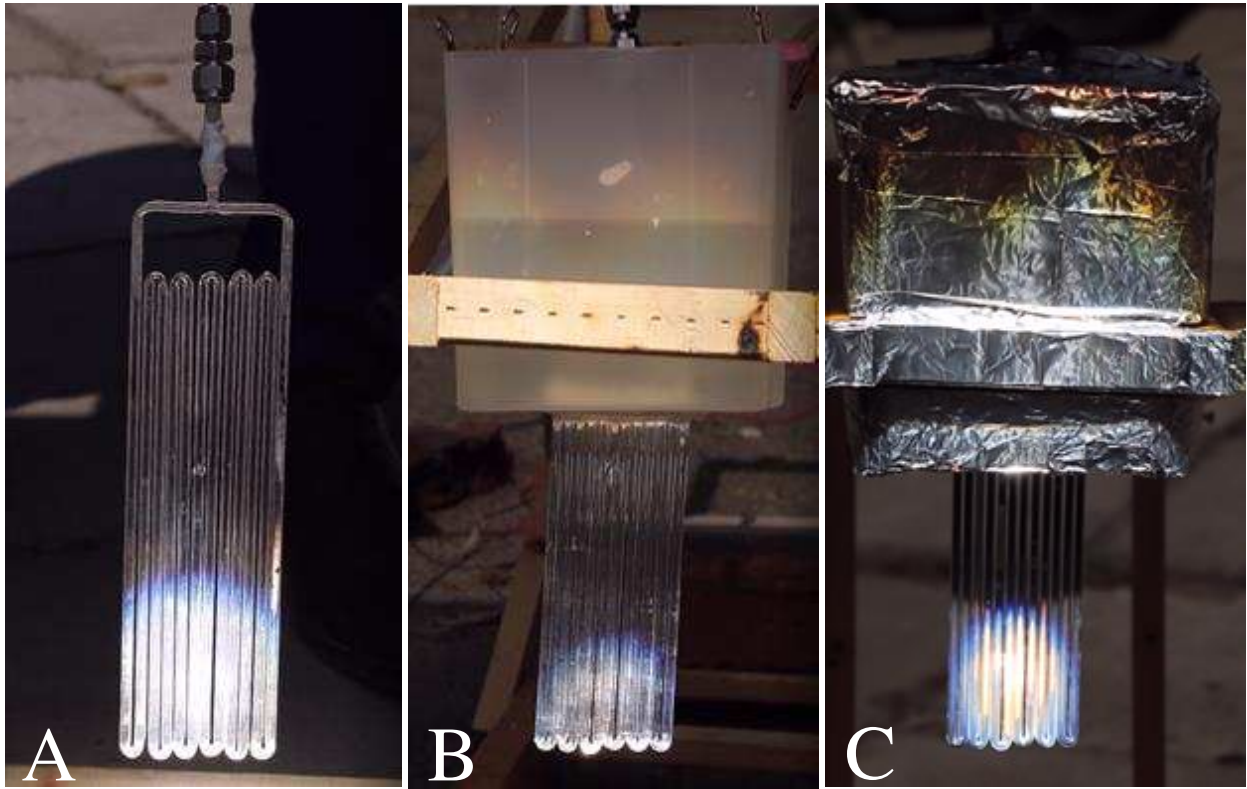
1
2
3



4

5 **Fig. 1** (A) TEM image for AuNPs; (B) SEM image and (C) TEM image for MWCNTs; (D) The
6 OHP with a gap of 1.5 mm between two adjacent pipes; (E) The OHP with no gap between two
7 adjacent pipes

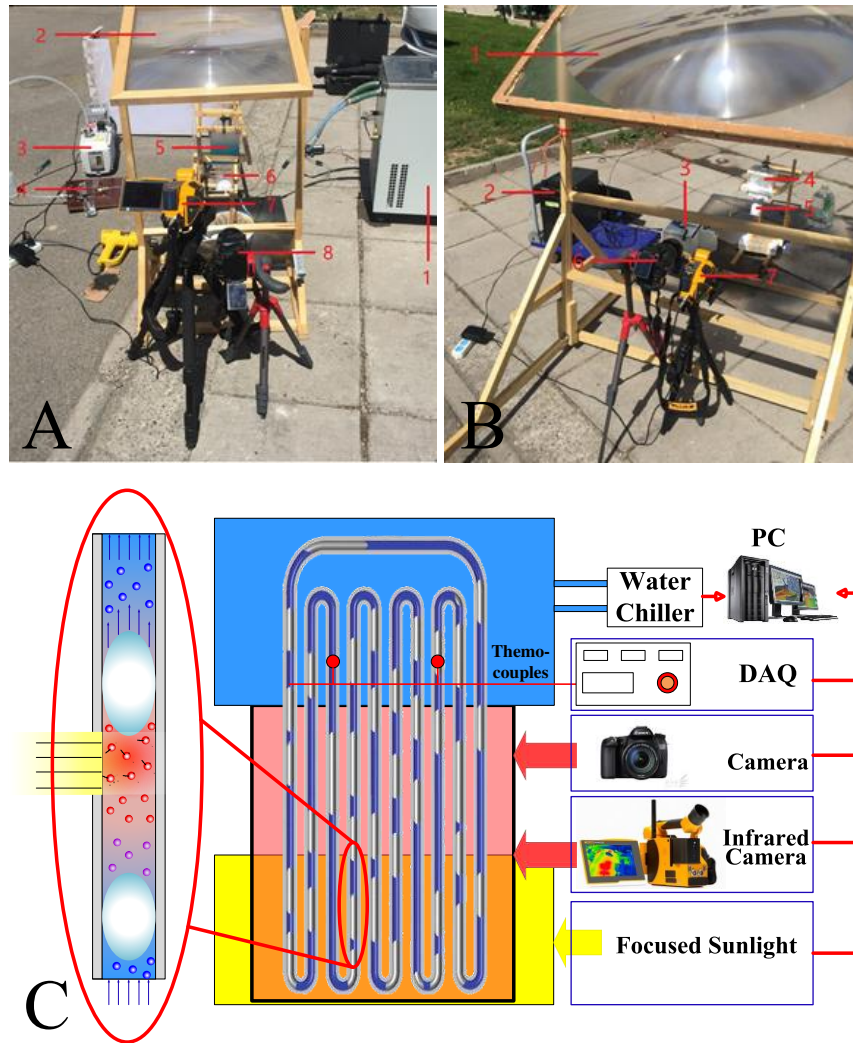
1
2
3
4
5
6
7
8
9
10



11
12
13
14

Fig. 2 Three types of OHP condenser cooling: (A) natural air convection; (B) circulating water cooling with constant temperature (5 °C or 15 °C); (C) 700 ml water tank with thermal insulation.

1

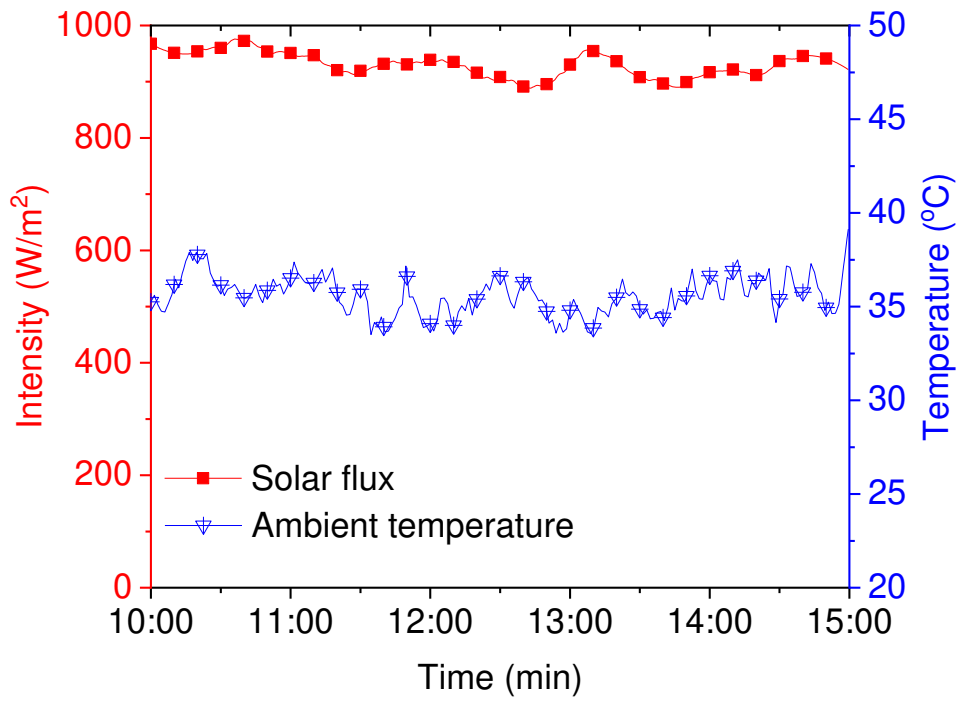


2

3 **Fig. 3** (A) Experimental system with circulating cooling water at the OHP condenser section: 1.
4 Refrigerator producing circulating cooling water with a constant temperature; 2. Fresnel lens with
5 the dimension of $0.5 \text{ m} \times 0.5 \text{ m}$; 3. Vacuum pump; 4. Filling pipeline for the OHP; 5. Cooling
6 water container maintaining at a constant temperature; 6. The OHP; 7. Infrared camera; 8. High-
7 speed camera; (B) Experimental system with a water tank at the OHP condenser section: 1. Fresnel
8 lens with the dimension of $1.1 \text{ m} \times 1.1 \text{ m}$; 2. The PC for displaying and recording the temperature
9 data; 3. Data acquisition system connected with three type K thermocouples; 4. Water tank

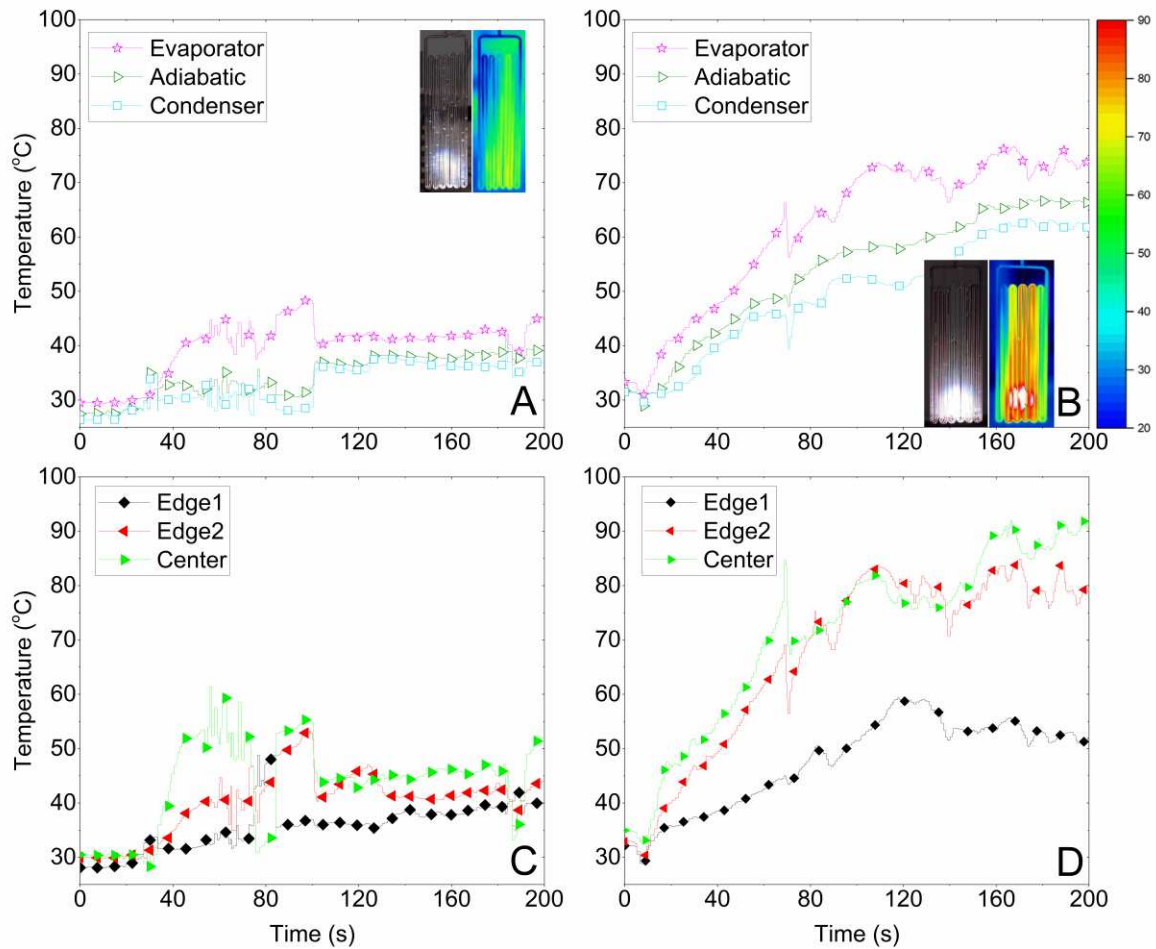
1 containing 700 ml water with thermal insulation; 5. The OHP; 6. High-speed camera; 7. Infrared
2 camera; (C) Schematic of the experimental system

3
4
5
6
7



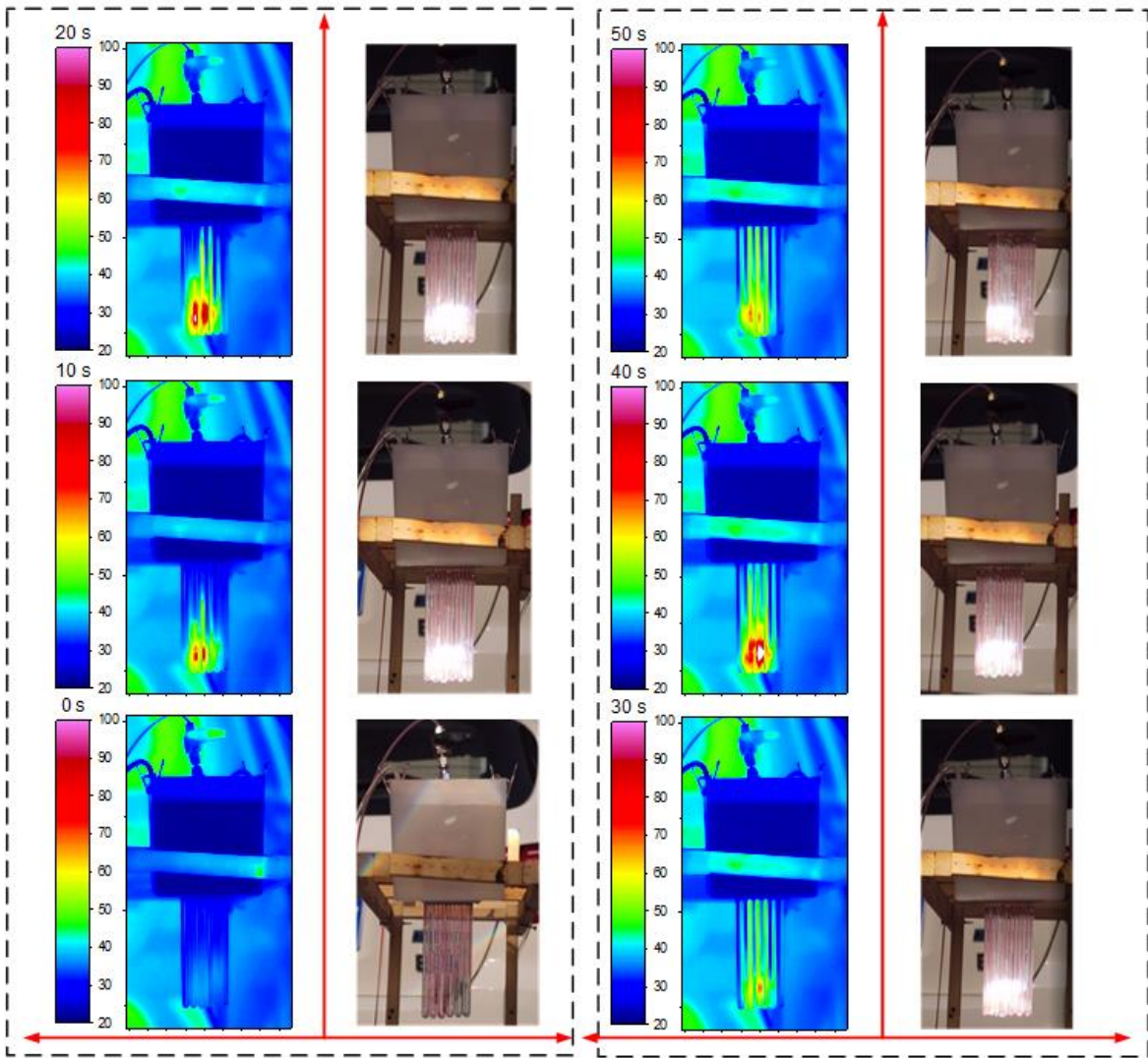
8
9
10
11
12
13
14
15

Fig. 4 Solar intensity and ambient temperature during experiment period



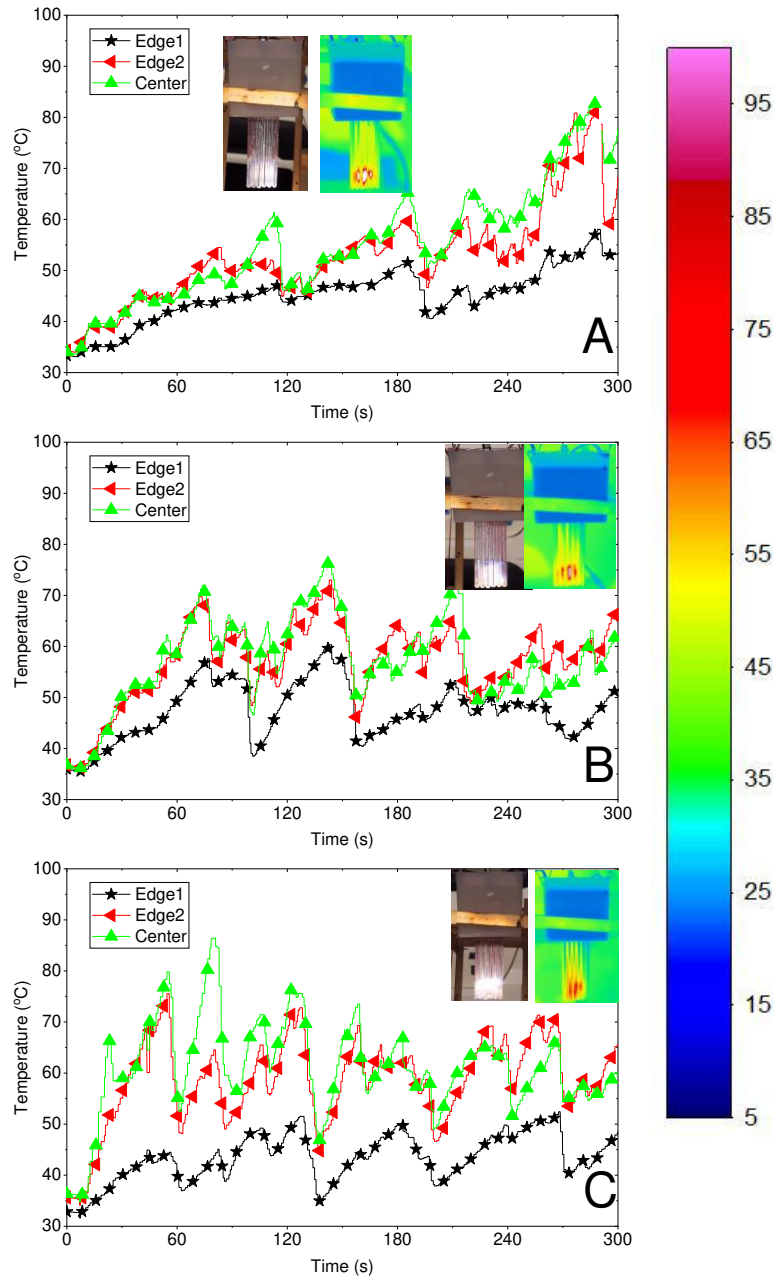
1
2 **Fig. 5** Temperature variations of the OHP with the filling ratio of 75% in **CASE (F)** and **CASE**
3 **(G)**: **(A)** and **(B)** show the average temperatures of the evaporator, adiabatic and condenser
4 sections of **CASE (F)** and **CASE (G)**, respectively; **(C)** and **(D)** show the temperature variations
5 at different positions (**Edge 1**, **Edge 2** and **Center**) at the evaporator section of **CASE (F)** and
6 **CASE (G)**, respectively. Insets of **(A)** and **(B)** show the visible and infrared images captured at
7 200 s.

8
9



1
 2 **Fig. 6** Infrared images and photos from high-speed camera of the OHP filled with 0.024 wt%
 3 AuNPs nanofluid and with the filling ratio of 83%
 4

1
2

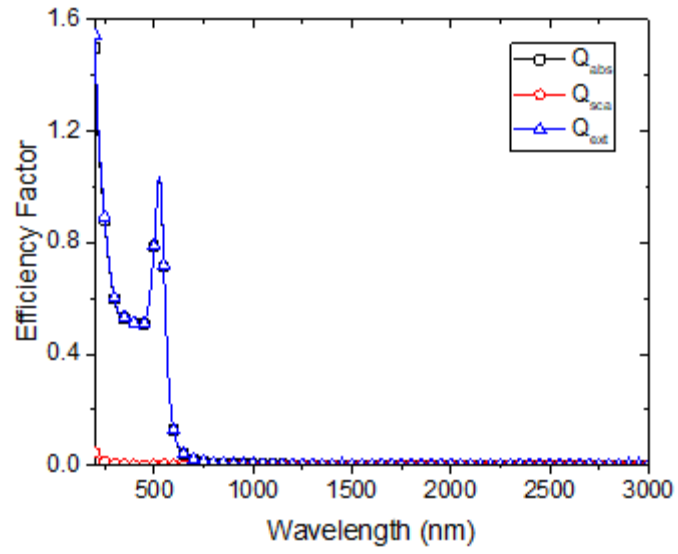


3

4 **Fig. 7** Temperature variation at the evaporator section for **CASE(C)** with different filling ratios:

5 (A) 42%; (B) 67%; and (C) 83%; The inset photos and infrared images are taken at 300 s

6



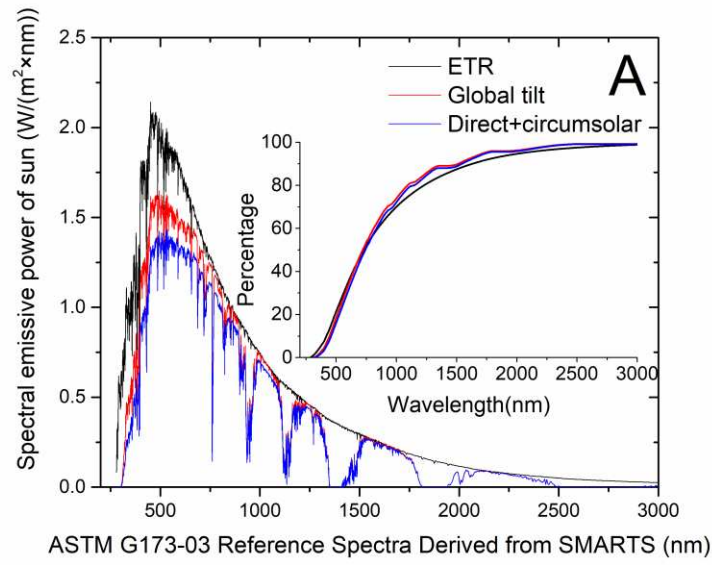
1

2

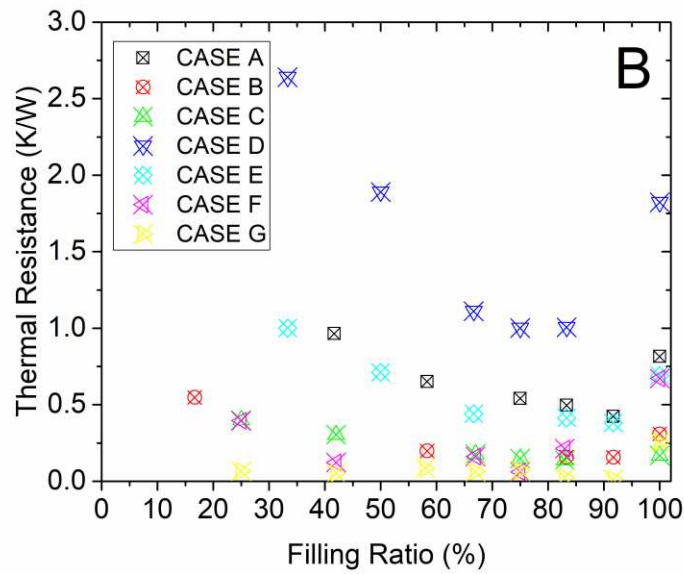
Fig. 8. Efficiency factors of gold nanoparticle with diameter of 20 nm.

3

4



1

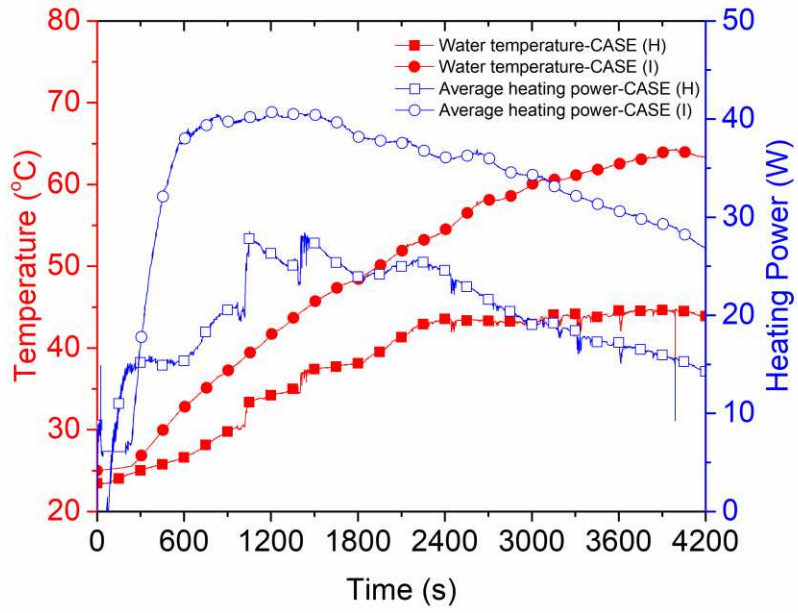


2

3 **Fig. 9 (A)** ASTM G173-03 Reference Spectra from the literature, the inset shows the solar energy
 4 distribution along with the wavelength in percentage (integrating spectral emissive power with the
 5 wavelength divided by irradiation intensity); **(B)** Variations of the thermal resistance with the
 6 filling ratio in different cases

7

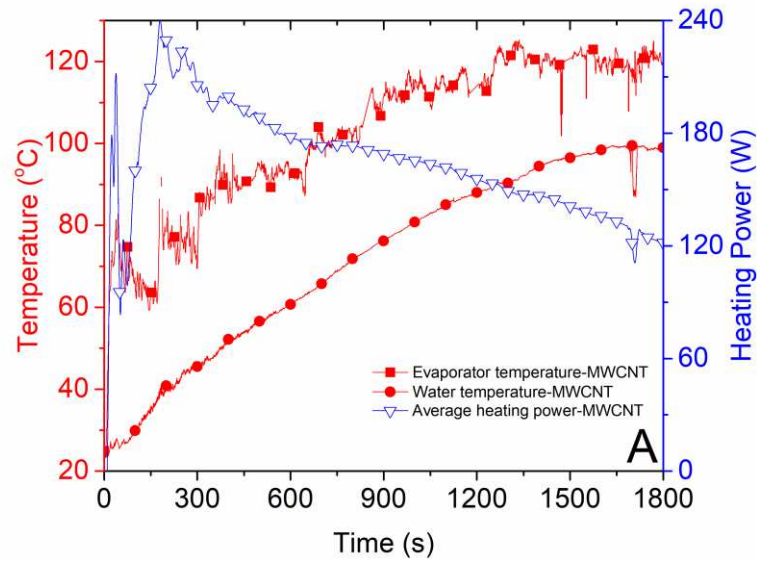
1
2
3
4
5



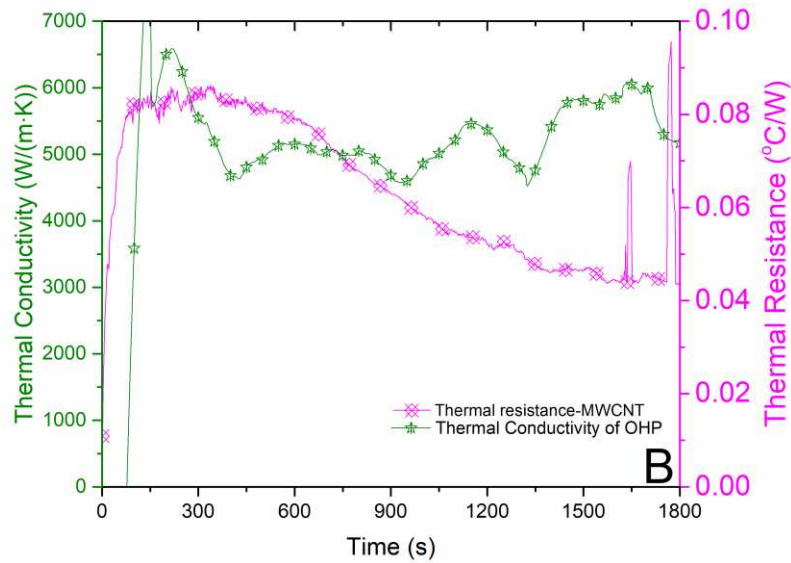
6
7
8

Fig. 10 Water temperature and average heating power variations in CASE (H) and CASE (I)

1
2



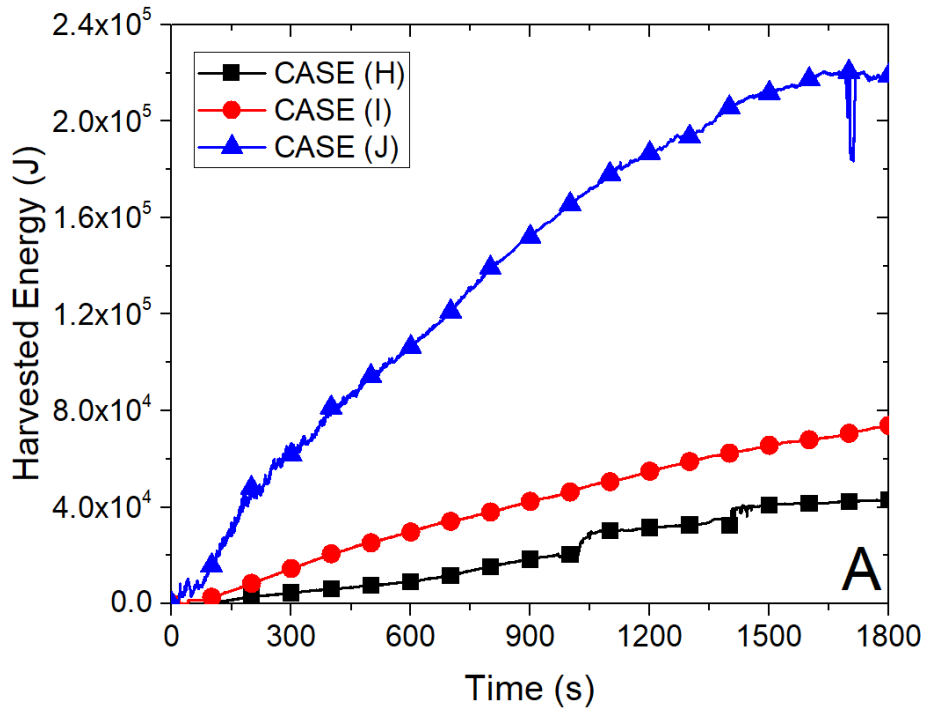
3



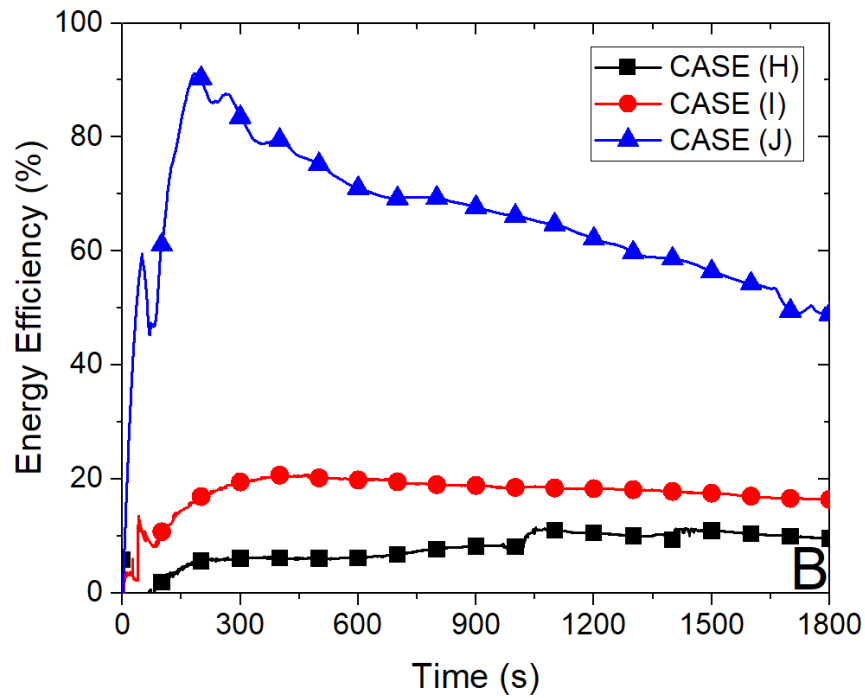
4

5 **Fig. 11 (A)** Evaporator temperature, water temperature and average heating power variations and
6 **(B)** thermal conductivity and thermal resistance variations of the OHP filled with MWCNT
7 nanofluid (**CASE J**), the filling ratio is 83%

8



1



2

3 **Fig. 12 (A)** Harvested energy and **(B)** energy efficiency of OHP filled with DI water (**CASE H**),
 4 0.024 wt% gold nanofluid (**CASE I**) and 3.0 wt % MWCNT nanofluid (**CASE J**), respectively
 5 (The filling ratio is 83%)